THE JOURNAL OF BIOLOGICAL CHEMISTRY VOL. 281, NO. 10, pp. 6273–6282, March 10, 2006

Importance of K^+-dependent Na^+/Ca^{2+}-exchanger 2, NCKX2, in Motor Learning and Memory*

Received for publication, November 11, 2005, and in revised form, January 5, 2006 Published, JBC Papers in Press, January 10, 2006, DOI 10.1074/jbc.M512137200

Xiao-Fang Li[‡§¶‖], Lech Kiedrowski[**], François Tremblay[‡‡], Fernando R. Fernandez[‡‖1], Marco Perizzolo[‖], Robert J. Winkfein[‖], Ray W. Turner[‡‖2], Jaideep S. Bains[‡‖3], Derrick E. Rancourt[¶§§4], and Jonathan Lytton[‡§¶‖4,5]

From [‡]The Hotchkiss Brain Institute, [§]Libin Cardiovascular Institute of Alberta, the [§§]Southern Alberta Cancer Research Institute, the [¶]the Department of Biochemistry and Molecular Biology, and the [‖]Department of Physiology and Biophysics, University of Calgary, Calgary, Alberta T2N 4N1, Canada, [**]The Psychiatric Institute, Departments of Psychiatry and Pharmacology, The University of Illinois, Chicago, Illinois 60612, and the [‡‡]Department of Ophthalmology & Visual Sciences, Dalhousie University, Halifax, Nova Scotia B3J 3G9, Canada

Plasma membrane Na^+/Ca^{2+}-exchangers play a predominant role in Ca^{2+} extrusion in brain. Neurons express several different Na^+/Ca^{2+}-exchangers belonging to both the K^+-independent NCX family and the K^+-dependent NCKX family. The unique contributions of each of these proteins to neuronal Ca^{2+} homeostasis and/or physiology remain largely unexplored. To address this question, we generated mice in which the gene encoding the abundant neuronal K^+-dependent Na^+/Ca^{2+}-exchanger protein, NCKX2, was knocked out. Analysis of these animals revealed a significant reduction in Ca^{2+} flux in cortical neurons, a profound loss of long term potentiation and an increase in long term depression at hippocampal Schaffer/CA1 synapses, and clear deficits in specific tests of motor learning and spatial working memory. Surprisingly, there was no obvious loss of photoreceptor function in cones, where expression of the NCKX2 protein had been reported previously. These data emphasize the critical and non-redundant role of NCKX2 in the local control of neuronal $[Ca^{2+}]$ that is essential for the development of synaptic plasticity associated with learning and memory.

Ca^{2+} ion plays a critical role in controlling a large number of neuronal processes, including neurotransmitter release, synaptic plasticity, neurite outgrowth, growth cone behavior, and apoptosis (1, 2). The specificity of Ca^{2+} signaling lies in complex spatial and temporal patterns mediated by the activity of membrane channels and transporters (3). Among these, Na^+/Ca^{2+}-exchange plays a predominant role in transporting Ca^{2+} across the plasma membrane. Under normal physiological conditions, the exchange process couples the electrochemical Na^+ gradient to the extrusion of Ca^{2+}. However, Na^+/Ca^{2+}-exchange can also catalyze Ca^{2+} influx under conditions in which the Na^+ gradient and/or the membrane potential are compromised (4). The role of Na^+/Ca^{2+}-exchange during pathological conditions such as ischemia is a controversial issue, with some studies suggesting a neuroprotective effect through enhanced Ca^{2+} extrusion, whereas others suggest a damaging effect due to exchanger-mediated Ca^{2+} influx (5–10).

The Na^+/Ca^{2+}-exchanger is encoded by a multigene superfamily of cation/Ca^{2+}-exchangers (11). In higher eukaryotes, genes from two branches of this superfamily encode Na^+/Ca^{2+}-exchangers: the NCX[6] (K^+-independent) exchangers, NCX1–3 (*SLC8A1–3*) and the K^+-dependent NCKX exchangers, NCKX1–4 (*SLC24A1–4*). The cardiac Na^+/Ca^{2+}-exchanger NCX1 is the best characterized member of the former, NCX, family (12), whereas the rod photoreceptor $Na^+/(Ca^{2+}+K^+)$-exchanger NCKX1 is the most extensively studied member of the latter, NCKX, family (13).

The pattern of expression of the NCX family members in brain has been characterized (14), and it is clear that NCX plays a key role in Ca^{2+} extrusion, particularly from synaptic sites in cultured hippocampal neurons (15). More recently, this role has been confirmed in mice lacking the NCX2 protein. Knock-out animals display reduced Ca^{2+} clearance from axon terminals and increased synaptic plasticity associated with enhancements in both learning and memory (16).

Gene products in the NCKX branch of the exchanger superfamily have only recently been identified and characterized. The expression of NCKX1 is restricted essentially to retina, whereas NCKX2, NCKX3, and NCKX4 are robustly and broadly expressed with distinct, but overlapping, regional distributions among brain neurons (17). Recent *in vitro* analysis has revealed an essential role for NCKX in calcium flux in cultured neurons (8, 18), and in Ca^{2+} extrusion from isolated axon terminals, particularly when $[Ca^{2+}]_i$ reaches μM levels or higher (19–21).

Although this growing evidence clearly demonstrates the importance of NCKX gene products in neuronal Ca^{2+} homeostasis, the unique contributions of NCKX-mediated Ca^{2+} transport to neuronal function *in vivo* have not yet been investigated. Moreover, in the context of so many different related gene products, the specific roles for any one isoform have not yet been defined. To address these issues, we used a gene-targeting approach to knock out expression of NCKX2, the major neuronally expressed isoform in this family. Mice lacking NCKX2 were analyzed molecularly, cellularly, and behaviorally, and found to exhibit deficits in neuronal Ca^{2+} homeostasis, in synaptic plasticity, and in measures of motor learning and memory.

EXPERIMENTAL PROCEDURES

Generation of NCKX2 Knock-out Mice—A mouse 129/SvJ genomic library (Stratagene) was probed with a PCR-derived fragment from exon

* This work was supported in part by operating Grant MOP15035 from the Canadian Institutes of Health Research (CIHR) (to J. L.), by National Institutes of Health Grant NS37390 (to L. K.), and by a CIHR operating grant (to R. W. T.). The costs of publication of this article were defrayed in part by the payment of page charges. This article must therefore be hereby marked "*advertisement*" in accordance with 18 U.S.C. Section 1734 solely to indicate this fact.

[1] Recipient of a CIHR Studentship.
[2] A Scientist of the Alberta Heritage Foundation for Medical Research.
[3] A Scholar of the Alberta Heritage Foundation for Medical Research.
[4] Senior Scholars of the Alberta Heritage Foundation for Medical Research.
[5] To whom correspondence should be addressed: University of Calgary Health Sciences Centre, Rm. 2518, 3330 Hospital Drive, NW, Calgary, Alberta T2N 4N1, Canada. Tel.: 403-220-2893; Fax: 403-283-4841; E-mail: jlytton@ucalgary.ca.

[6] The abbreviations used are: NCX, Na^+/Ca^{2+}-exchanger (K^+-independent) gene family, SLC8; NCKX, $Na^+/(Ca^{2+}+K^+)$-exchanger gene family, SLC24; BK, large conductance Ca^{2+}-activated K^+ channel; fEPSP, field excitatory post-synaptic potential; LTD, long term depression; LTP, long term potentiation; NMDA, *N*-methyl-D-aspartate; SK, small conductance Ca^{2+}-activated K^+ channel; cd, candelas; SERCA, sarcoplasmic or endoplasmic reticulum Ca^{2+}-ATPase.

2 of mouse *nckx2* to yield clones spanning a genomic region of ~15 kb encompassing only exon 2. A targeting construct was engineered by combining two contiguous ~3-kb HindIII genomic fragments with a polymerase II promoter-driven neomycin resistance cassette (22), and the herpes simplex virus promoter-driven thymidine kinase gene derived from the pflox vector (23), to create the molecule illustrated in Fig. 1*A*, in which the neomycin resistance gene has been inserted in the antisense orientation into the unique HindIII site within exon 2, while the thymidine kinase gene flanks the 5′ end of the upstream *nckx2* fragment. An NotI fragment of ~11 kb was isolated and used to electroporate R1 embryonic stem cells, which were subjected to positive-negative selection as previous described (22). Targeted cells were identified by Southern blot using an upstream ApaI-HindIII probe. Positive clones were expanded, karyotyped, and re-screened to confirm the targeted locus before being used for blastocyst injections to create chimeric mice, as previously described (24). Male chimeras were then bred with C57Bl/6 females, and agouti animals screened by Southern blot to identify recombinant *nckx2*(+/−) heterozygous animals. Subsequent animal genotyping was conducted using a mixed PCR primer protocol. Most studies were performed on F2 animals from *nckx2*(+/−) heterozygote crosses, using littermates of different genotypes for comparison. In some experiments, particularly the brain slice electrophysiology, *nckx2*(+/−) heterozygote animals derived from more than ten C57Bl/6 backcrosses were bred to generate the (+/+) and (−/−) littermates studied. Embryonic stem cell targeting and chimeric mice production were conducted at the Center for Mouse Genomics, Faculty of Medicine, University of Calgary. Mice were maintained and treated in accordance with the guidelines of the Canadian Council on Animal Care as determined by the University of Calgary Animal Care Committee. Mice were sacrificed for all experiments described below following halothane anesthesia.

Molecular Analyses—All molecular biology procedures were conducted essentially according to standard protocols (25). Genotyping of mice was performed using genomic DNA isolated by phenol:chloroform extraction and ethanol precipitation from either tail or ear-punch biopsies. For Southern analysis, DNA was digested overnight with EcoRI, separated on a 0.8% agarose gel, transferred to nylon, and probed with a digoxigenin-labeled genomic fragment found upstream of the targeting sequence. This probe recognizes an 11-kb band in genomic DNA from wild-type *nckx2*, and an 8-kb band in the targeted allele (Fig. 1*A*). For PCR analysis, we employed forward (P2, GGCATGTGTGCTCTGTTTTCTA) and reverse (P1, CCACATAGGCGAAATAAGCTGT) primers from within exon 2 of mouse *nckx2* and forward primer from the neomycin resistance cassette (P3, CGGGCCTCGTTCATGAATATTC; this primer is actually found as the reverse complement of sequences from the murine polymerase II promoter at the 5′-end of the neomycin resistance cassette). Amplification from wild-type genomic DNA resulted in a band of 172 nucleotides between primers P1 and P2, whereas amplification from the targeted locus resulted in a band of 283 nucleotides between primers P1 and P3 (see Fig. 1*A*).

Total cellular RNA was isolated from whole brain or eyes of 4- to 5-month-old mice of different genotype by guanidinium isothiocyanate extraction and CsCl centrifugation. 10 μg of total RNA was separated by formaldehyde-agarose electrophoresis, transferred to nylon, and analyzed at high stringency essentially as described previously (26) using digoxigenin-labeled probes corresponding to nucleotides 379–1102 of rat nckx2 exon 2 (5′ probe) or nucleotides 5004–8086 of exon 12 (3′ probe), nucleotides 11–1376 of rat nckx1, nucleotides 259–1846 of mouse nckx3, nucleotides 680–1398 of mouse nckx4, nucleotides 1815–3290 of rat ncx1, nucleotides 1016–1907 of rat ncx2, or nucleotides 1–1273 of rat gapdh.

A membrane fraction, enriched in synaptic markers, was isolated from homogenized whole brains of mice of each genotype according to published procedures (27). Aliquots of 5 μg of this membrane fraction were separated by SDS-PAGE (28), transferred to nitrocellulose membranes, and probed with antibodies against either NCKX2 (polyclonal PA-926 (from Affinity BioReagents, Inc.), polyclonal N2F (29), and monoclonal A6F3 (N2F and A6F3 were prepared at the Southern Alberta Cancer Research Center Hybridoma and Antibody Facility by immunizing rabbits or mice with a glutathione *S*-transferase fusion protein encoding amino acids 384–463 of rat NCKX2; N2F was affinity-purified using a parallel maltose-binding protein-fusion)), NCX1 (monoclonal antibody R3F1 (30)), the plasma membrane Ca-ATPase (monoclonal antibody 5F10 (from Affinity BioReagents, Inc.)), or sarcoplasmic or endoplasmic reticulum Ca^{2+}-ATPase (SERCA) Ca^{2+} pump (polyclonal antibody N (31)).

Morphological Analyses—Mice were transcardially perfused with 4% paraformaldehyde in 0.1 M sodium phosphate buffer, pH 7.4, and the brain was removed and fixed overnight in the same solution. For histological analysis, brains were then embedded in paraffin, and 8-μm parasagittal sections were cut and stained with hematoxylin and eosin by standard procedures. Immunofluorescence was performed on 50-μm free floating brain horizontal sections cut by using a vibratome. The sections were blocked for 1 h in working solution (3% donkey serum, 2% dimethyl sulfoxide, and 0.2% Tween 20 in 0.1 M sodium phosphate buffer, pH 7.4), then incubated at 4 °C overnight with affinity-purified polyclonal N2F antibody diluted 1:1000 in working solution. After three rinses with working solution diluted 1:3 with 0.1 M sodium phosphate buffer, the sections were incubated at 4 °C overnight with Cy3-conjugated donkey anti-rabbit antibody diluted 1:1000 in working solution. After three more washes with 0.1 M sodium phosphate buffer, the sections were mounted on slides, observed with a 63× oil-immersion objective on a Zeiss Axioskop 2 microscope, and photographed using a SPOT RT-Slider camera (Diagnostic Instruments, Inc.). Exposure and contrast of the photographs (adjusted using Adobe Photoshop CS) from the *nckx2*(−/−) animal sections were the same as those used to photograph and adjust the wild-type sections.

Eyes from 10-week-old mice were fixed in 4% paraformaldehyde in phosphate buffered saline at room temperature for 2 h, cryoprotected by soaking in 30% sucrose solution, and embedded in OCT. 11-μm cryostat sections were mounted on glass slides, blocked, and permeabilized with 10% normal goat serum, 0.3% Triton X-100 in phosphate-buffered saline, and then analyzed using either the M/L-cone-specific antibody, COS-1 (32) followed by Alexa488-conjugated anti-mouse secondary antibody, or with rhodamine-conjugated peanut agglutinin-lectin, which specifically recognizes cone outer segment sheaths (33). Labeled eye sections were observed and photographed as described above.

Neuronal Cell Culture and Ca^{2+} Imaging—Primary cultures of cortical neurons were prepared from new born mouse pups obtained either from *nckx2*(−/−) or *nckx2*(+/+) breeding pairs, which were each the littermate progeny of *nckx2*(+/−) matings. Neurons were grown and maintained in culture for 14–17 days as described previously (8). To monitor Ca^{2+} fluxes associated with the reverse action of NCKX exchangers, cells were first loaded with the Ca^{2+} indicator Fura-FF (using the acetoxymethyl ester obtained from Teflabs) and then incubated in 96.7 mM NaCl, 3.6 mM $NaHCO_3$, 5 mM KCl, 57.9 mM *N*-methyl-D-glutamine-Cl, 1.3 mM $CaCl_2$, 1 mM $MgCl_2$, 10 mM HEPES-Tris, pH 7.4, containing 1 mM ouabain, 10 μM nifedipine, 10 μM 2,3-dioxo-

6-nitro-1,2,3,4-tetrahydrobenzo[*f*]quinoxaline-7-sulfonamide (NBQX), 10 μM (5*S*,10*R*)-(+)-5-methyl-10,11-dihydro-5H-dibenzo[*a*,*d*]cycohepten-5,10-imine (MK-801), 1 mM iodoacetate, 2 μM rotenone, 3 μg/ml oligomycin, and 10 μM KB-R7943. These conditions were chosen to inhibit all other pathways for calcium entry and to block the production of cellular ATP that will drive ATP-dependent Ca^{2+} sequestration and efflux pathways. The accumulation of [Ca^{2+}] that is a measure of exchanger-dependent Ca^{2+} flux is compromised if any of these inhibitors are not present (8, 34, 35). In some experiments (Fig. 4*E*), a K^+-free medium was used. This medium had the same composition as that described above except KCl was omitted and NaCl and *N*-methyl-D-glutamine-Cl concentrations were increased to 100 and 59.6 mM, respectively. Ca^{2+} uptake via NCKX was then initiated by equilibrating the plasma membrane Na^+ gradient using 5 μM gramicidin. The change in [Ca^{2+}] was monitored by measuring the fluorescence emitted by neuronal cell bodies excited at either 340 or 380 nm using an Attofluor digital imaging system fitted to a Zeiss Axiovert 100 microscope. Calibration and conversion from fluorescence units to Ca^{2+} flux, measured in micromolar/min was performed as described previously (8). Under these conditions, more than 90% of the resulting Ca^{2+} flux is dependent upon external K^+, consistent with the requirements of NCKX for activity (see Fig. 4*E*).

Brain Slice Electrophysiology—Hippocampal slices (400-μm thickness) of *nckx2*(+/+) or *nckx2*(−/−) age-matched littermates (8–9 weeks old for LTP measurements and 3–4 weeks old for LTD measurements) were prepared in ice-cold high sucrose slicing solution (87 mM NaCl, 1.25 mM NaH_2PO_4, 2.5 mM KCl, 25 mM $NaHCO_3$, 0.5 mM $CaCl_2$, 7 mM $MgCl_2$, 25 mM glucose, and 75 mM sucrose, pH 7.4) saturated with 95% O_2/5% CO_2, and then incubated in artificial cerebrospinal fluid (126 mM NaCl, 1.25 mM NaH_2PO_4, 2.5 mM KCl, 26 mM $NaHCO_3$, 2 mM $CaCl_2$, 2 mM $MgCl_2$, and 10 mM glucose, pH 7.4) saturated with 95% O_2/5% CO_2 for at least 1 h at 35 °C prior to recording at 25 °C. Extracellular field potentials were recorded in the stratum radiatum area of CA1 neurons using a glass recording microelectrode filled with artificial cerebrospinal fluid (3- to 5-MΩ resistance). Synaptic responses were elicited by stimulation of the Schaffer collateral fibers using a monopolar platinum stimulating electrode (grounded to the bath) placed in the stratum radiatum area close to the CA2 region, ~100 μm from the glass recording microelectrode. A series of test responses were elicited to determine a baseline stimulation intensity that corresponded to ~50% of the maximum evoked response. fEPSPs were then recorded at 0.1 Hz for 10 min. LTP was initiated with two 0.5-s, 100-Hz stimulation trains, and LTD was invoked by 15 min of 1-Hz stimulation. fEPSPs recordings were continued at 0.1 Hz for 30–45 min following initiation of either LTP or LTD. Traces were acquired using a Digidata 1340 interface, recorded with an Axopatch 200B amplifier, and analyzed using Clampfit software (Axon Instruments, Inc.). The fEPSP slope was calculated from the rising phase (10–90%) of the peak response.

For whole cell current-clamp analysis of CA1 pyramidal neurons, hippocampal slices cut as described above were transferred into buffer composed of 125 mM NaCl, 3.25 mM KCl, 1.5 mM $CaCl_2$, 1.5 mM $MgCl_2$, 25 mM $NaHCO_3$, and 25 mM D-glucose, and saturated with 95% O_2, 5% CO_2, placed in the recording chamber of a Zeiss Axioskop FS-2 microscope, and maintained at 22 °C as a submerged preparation. Neurons were visualized using differential interference contrast optics and infrared light transmission. All recordings were carried out in the presence of synaptic blockers that were bath-applied after obtaining the initial seal: 50 μM picrotoxin, 25 μM DL-2-amino-5-phosphonopentanoic acid, 10 μM 6,7-dinitroquinoxaline-2,3-dione, and 1 μM CGP 55845. Pipettes had a resistance of 4–8 MΩ with access resistance of 8–15 MΩ. Our internal solution for current clamp recordings consisted of 130 mM potassium gluconate, 0.1 mM EGTA, 10 mM HEPES, 7 mM NaCl, 0.3 mM $MgCl_2$, 5 mM di-tris-creatine phosphate, 2 mM Tris-ATP, and 0.5 mM sodium GTP, pH 7.3, with KOH. Membrane potential was then recorded in response to 300-ms current injection pulses stepping from −60 pA to +185 pA in 5-pA increments. Data were collected using a Multiclamp 700A amplifier and pClamp 8.1 software (Axon Instruments, Inc.).

Behavioral Assessment—A battery of behavioral tests, including appearance and reflexes and tests of sensorimotor functions, visual and auditory perception, learning, and memory, were conducted by Neuro-Investigations, Inc. at the Canadian Centre for Behavioral Neuroscience at the University of Lethbridge, Alberta, Canada, according to established procedures (36). Twelve 4- to 5-month-old, age-matched littermate mice, six female and six male, of each genotype (wild-type and *nckx2* knock-out) were tested. The accelerating rotating rod (rotarod) task consists of a 5-cm round drum suspended between Plexiglas walls 24 cm above a soft mat. Mice were subjected to two three-trial sessions, one session per day. For each trial the mice were first placed on the stationary rod for 1 min. At that point, the rod was rotated at 5 rpm for 1 min, and subsequently the speed increased in 5-rpm increments each minute until the mouse fell off, or 50 rpm was reached. The speed of the rod at which the mice fell off was then averaged for each session and genotype. The Morris water maze task hidden platform test was performed by placing the mice into a round pool of opaque water from one of four different peripheral start locations. The mice were allowed to swim about within the pool for 60 s to locate a platform hidden just beneath the surface of the water. The platform remained in the same location throughout the test. Distal clues to orientation were provided on the four walls of the room, visible above the level of the water through the Plexiglas walls of the pool, but there were no local cues within the pool. Each mouse was given a block of four trials with 10 min between each trial, twice a day for 7 days. The time required to find the platform was averaged over the four trials within each block and recorded. In the moving platform version of the Morris water maze task, mice were first given a block of 4 trials once per day for 4 days during which the hidden platform was moved to a novel location on each day. On the subsequent 6 test days, the platform was left in the same position for 2 days at a time, such that on days 5, 7, and 9 the platform was in a novel location, but on days 6, 8, and 10, the platform was in the same location as it had been on the previous day. A block of four test trials was administered on each day. The time taken during each test trial to find the platform in either the novel or the same location was then averaged for all the mice within each genotype across the test days.

Electroretinography—Mice were dark-adapted for at least 60 min and anesthetized, and retinal recordings were obtained essentially as described previously (37). Scotopic recordings were obtained by stimulating from complete darkness with a series of light flashes of increasing intensity, spanning 4.8 log units up to a maximum flash intensity of 10 cd·s/m^2 in steps of 0.4 log units using an interstimulus rate of 0.3 Hz or lower. Recordings in photopic conditions were performed after 10 min of exposure to a white background intensity of 32 cd/m^2. Flashes of intensity ranging from 0.6 to 10 cd·s/m^2 were then delivered at a rate of 0.9 Hz.

Statistics—Data are presented in all plots as the means ± S.E. Differences between genotypes were tested either using the *t* test statistic, one-way or two-way analysis of variance followed by Bonferroni post-test analysis, or the Mann-Whitney rank sum test. Statistically significant differences was accepted with p values of <0.05.

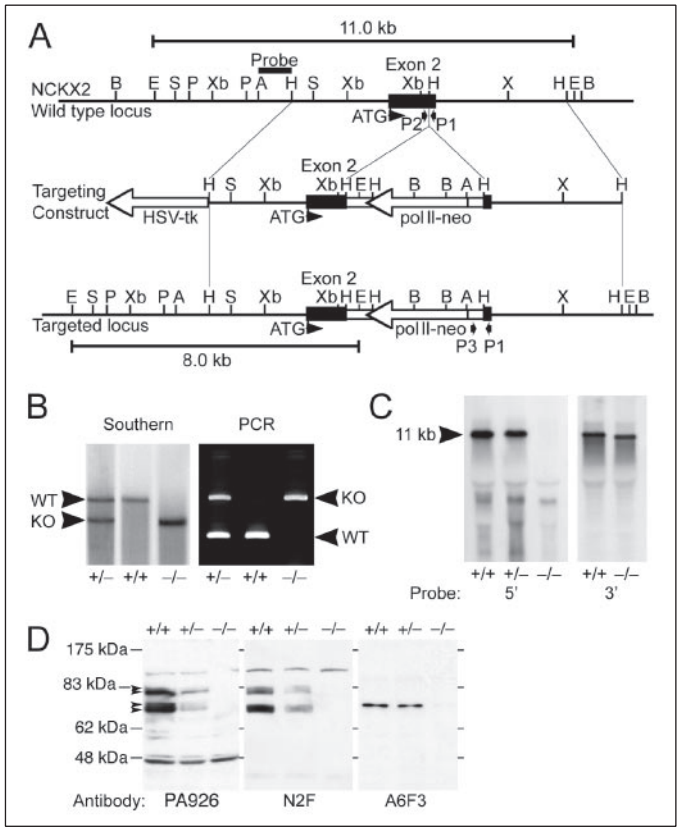

FIGURE 1. **Generation of *nckx2* knock-out mice.** *A*, diagram of the relevant region of the *nckx2* gene, the targeting vector, and the targeted locus. The location of *nckx2* exon 2, which contains the protein start codon (ATG), is shown by a *closed box*, and the neo cassette used to disrupt it is shown by a *large open arrow*. The location of the probe used for Southern analysis is indicated with a *bar*, and the size of the EcoRI fragments this probe recognizes are shown. *Small arrows* labeled *P1*, *P2*, and *P3* illustrate the location of primers used for PCR analysis of genotype. *A*, ApaI; *B*, BamHI; *E*, EcoRI; *H*, HindIII; *P*, PstI; *S*, SpeI; *X*, XhoI; *Xb*, XbaI. *B*, genotype analysis on biopsy sample DNA from *nckx2* heterozygous (+/−), wild-type (+/+), or knock-out (−/−) animals, was performed by Southern blot of EcoRI-digested DNA, or by ethidium bromide staining of PCR products. *C*, Northern analysis of *nckx2* transcripts present in 10-μg samples of brain total RNA from *nckx2*(+/+), *nckx2*(+/−), and *nckx2*(−/−) animals. Note the absence of the 11-kb band when the blot was analyzed with a probe from within exon 2 (5′), and the generation of a smaller *nckx2* transcript when the blot was analyzed with a probe from the 3′-end of the gene. *D*, immunoblots of 5-μg samples of a membrane fraction from whole brains of *nckx2*(+/+), *nckx2*(+/−), and *nckx2*(−/−) mice analyzed with three different antibodies directed against NCKX2.

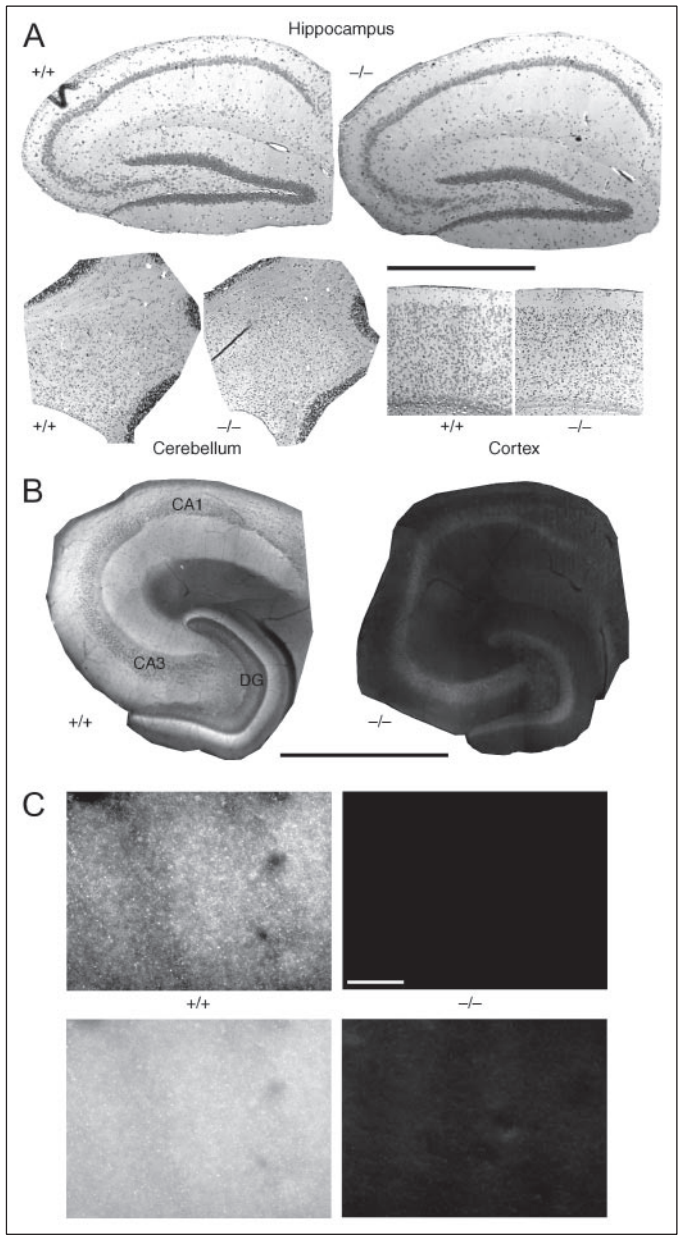

FIGURE 2. **Brain morphology and NCKX2 expression.** *A*, morphology of *nckx2* wild-type (+/+) and knock-out (−/−) brains is illustrated with hematoxylin-eosin-stained parasagittal sections corresponding to the indicated regions. *Scale bar*, 1.0 mm. *B*, horizontal sections from hippocampus of *nckx2* wild-type (+/+) and knock-out (−/−) mice were labeled with affinity-purified N2F anti-NCKX2 polyclonal antibody. Note that N2F has a slight nonspecific reactivity within the cell body layer of CA1, CA3, and dentate gyrus, visible in the (−/−) section. *Scale bar*, 1.0 mm. *C*, an enlargement of the stratum radiatum layer from the CA1 region of hippocampus. *Scale bar*, 20 μm. Contrast on the *upper pair of images* has been enhanced to emphasize the punctate appearance of N2F staining, whereas in the *lower pair of images* it has been adjusted to reveal the background present in the (−/−) image. For each of the wild-type and knock-out pairs shown in *B* and *C*, both images were acquired with the same exposure settings, and their contrast was adjusted in parallel using the same settings.

RESULTS

NCKX2 Knock-out—The mouse *nckx2* gene was disrupted as illustrated in Fig. 1. The expression of the 11-kb *nckx2* transcript in brain RNA was analyzed by Northern blot with probes from either the 5′-end (exon 2; nucleotides 379–1102) or the 3′-end (probe from exon 12; nucleotides 5004–8086). As illustrated in Fig. 1*C*, although the *nckx2* transcript was still detected with the 3′-end probe, the size of the band was slightly smaller in brain RNA from the knock-out animals as compared with wild type. The shift in size is due to the exclusion of the disrupted exon 2 from the transcript, because blots with the exon 2 probe revealed complete loss of signal in the knock-out animals (Figs. 1*C* and 3*A*).

Transcription of the *nckx2* gene is known to begin at several sites resulting in the incorporation of alternative first exons within the 5′-untranslated region of the transcript (38). Exon 2 encodes the first 360 amino acids (more than half) of the NCKX2 protein. Without the first half of the coding region, the NCKX2 protein cannot be expressed, as demonstrated by immunoblots probed with antibodies directed against epitopes either within (PA926) or downstream (N2F and A6F3) of exon 2-encoded sequence (Fig. 1*D*). Note that antibodies PA926 and N2F both recognized a pair of doublet bands that were specific to NCKX2. The differently sized bands are probably the products of alternatively spliced transcripts, one described previously (39), and one newly identified in mouse (data not shown). A6F3 bound an epitope that must overlap with the 17-amino acid segment encoded by the alternatively spliced exon described previously (39), because this antibody recognized the upper band in each doublet (although only one band is clearly

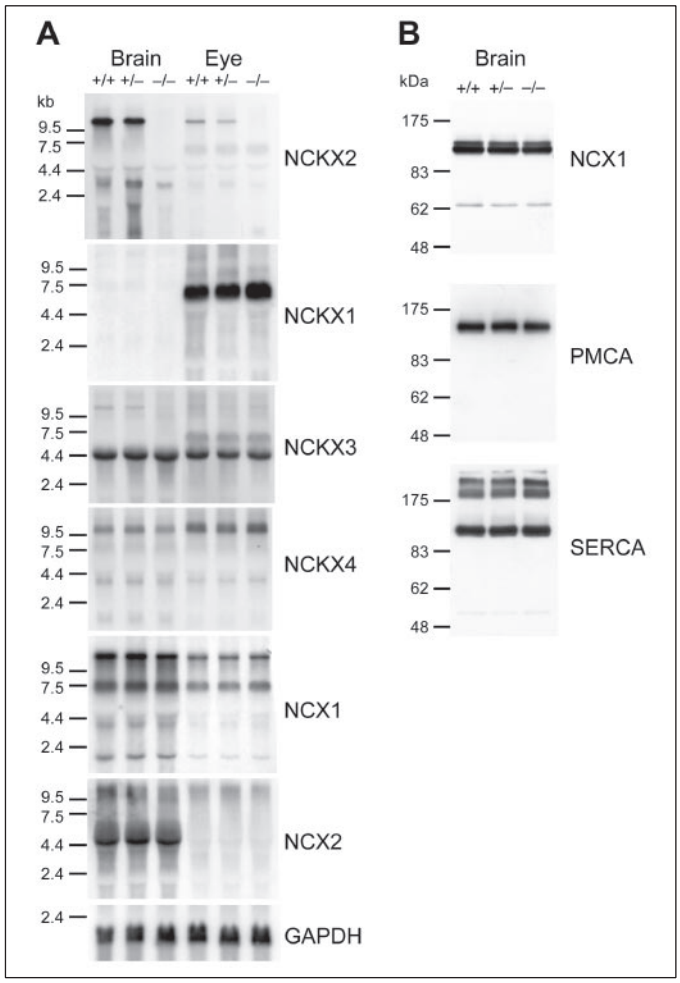

FIGURE 3. **Expression of other Ca^{2+} transporters.** *A*, Northern blots of 10-μg samples of total RNA isolated from either brain or eye of *nckx2*(+/+), *nckx2*(+/−), and *nckx2*(−/−) mice, were analyzed with probes from the indicated gene products at high stringency. The 5′ exon 2 probe was used for the nckx2 blot, and the *brain lanes* are the same as shown in Fig. 1. *GAPDH*, glyceraldehyde-3-phosphate dehydrogenase, used as a loading control. *B*, immunoblots of 5-μg samples of a synaptic-marker enriched membrane fraction isolated from whole brains of *nckx2*(+/+), *nckx2*(+/−), and *nckx2*(−/−) mice analyzed with antibodies against NCX1, the plasma membrane Ca^{2+}-ATPase (*PMCA*) and the SERCA Ca^{2+}-ATPase (*SERCA*). Note that the *upper two bands* (above the 175-kDa marker) observed with the anti-SERCA antibody correspond to aggregated material, probably induced during the membrane isolation and/or storage procedure.

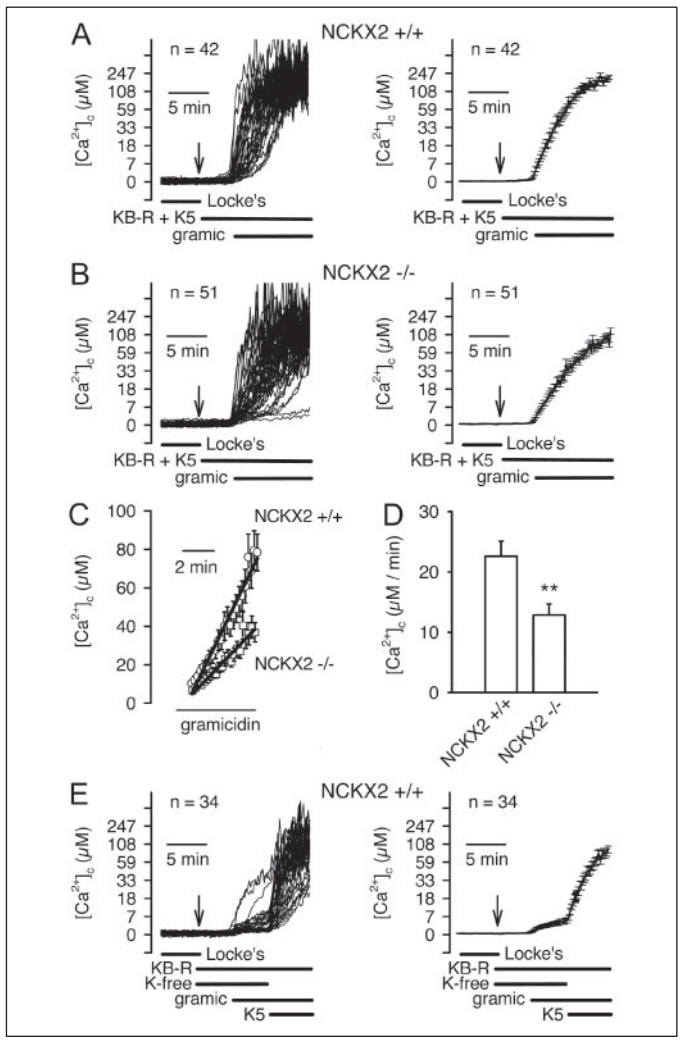

FIGURE 4. **NCKX-mediated Ca^{2+} entry into cultured cortical neurons.** *A* and *B*, Ca^{2+}-entry via plasma membrane K^+-dependent Na^+/Ca^{2+}-exchangers was initiated by the addition of 5 μM gramicidin (*gramic*) to equilibrate the Na^+ gradient, and monitored by Fura-FF fluorescence, in cortical neurons cultured from *nckx2* wild-type (+/+) or knock-out (−/−) mice. Ca^{2+} flux via pathways other than K^+-dependent Na^+/Ca^{2+}-exchangers was prevented by the addition, at the *arrow*, of medium containing a mixture of various inhibitors (see "Experimental Procedures"), including the NCX inhibitor KB-R7943 (*KB-R*) plus 5 mM KCl (*K5*). In each *panel* the *left plot* shows individual traces (fluorescence data converted to $[Ca^{2+}]$) obtained from the indicated number of cells in one microscopic field, whereas the *right plot* shows averaged data. *C*, a portion of the data from *A* and *B* has been replotted on a linear scale to illustrate the linear regression fit used to calculate the rate of gramicidin-induced $[Ca^{2+}]$ rise. *D*, summary data for the rate of $[Ca^{2+}]$ rise obtained from 15 experiments on four different neuronal cultures for each genotype. **, $p < 0.01$ (Mann-Whitney rank sum test). *E*, the K^+ dependence of Ca^{2+} entry into *nckx2* wild-type cortical neurons, measured as described above for *A* and *B*, except that incubation solutions initially lacked KCl, which was then added back at a concentration of 5 mM (K5). Under the conditions used for these experiments, more than 90% of the rate of $[Ca^{2+}]$ rise depends upon the presence of K^+.

evident in the exposure shown in Fig. 1). These data confirm that targeting of the *nckx2* gene resulted in a null allele for this locus.

Mice lacking the NCKX2 protein were viable, fertile, and morphologically indistinguishable from their wild-type litter mates (data not shown). In addition, histological analysis of brain morphology by hematoxylin-eosin staining did not reveal any obvious differences (Fig. 2*A*). Importantly, there was no significant difference in number or morphology of hippocampal pyramidal cells, where the *nckx2* transcript is abundant (39). Sections from hippocampus were stained with affinity-purified anti-NCKX2 polyclonal antibody N2F (Fig. 2, *B* and *C*), which revealed a punctate pattern of expression most evident in the oriens, stratum radiatum, and dentate gyrus molecular layers, that was absent from the knock-out animals. Staining in the pyramidal cell layer was not different between wild-type and knock-out samples and corresponded to slight nonspecificity of the polyclonal antibody. This staining pattern suggested that the NCKX2 protein was concentrated at synaptic sites, but not in the cell soma, of hippocampal pyramidal neurons.

We investigated if the loss of NCKX2-mediated Ca^{2+} extrusion might be compensated by an increase in the expression of other Ca^{2+} transporters. RNA isolated from brain and eye of wild-type, heterozygous, and knock-out animals was analyzed by Northern blot for expression of the Na^+/Ca^{2+}-exchanger genes *nckx1*, *nckx3*, *nckx4*, *ncx1*, and *ncx2*. In addition, a membrane fraction from brain was examined by immunoblot for the NCX1 protein, the plasma membrane Ca^{2+}-ATPase protein, and the SERCA Ca^{2+} pump. In all cases, there was no significant change in the expression of these other Ca^{2+} transport proteins or their transcripts (Fig. 3).

Neuronal Ca^{2+} Flux—NCKX activity was assessed in cultured neurons from the cerebral cortex of newborn *nckx2* wild-type or knock-out animals as the K^+-dependent, KB-R7943-independent, rise in the concentration of intracellular Ca^{2+} ($[Ca^{2+}]_i$) upon equilibration of the Na^+

gradient by gramicidin, as illustrated in Fig. 4 (8, 18). Treatment with KB-R7943, to inhibit Ca^{2+} entry through NCX exchangers and thus reveal NCKX activity, reduced Ca^{2+} influx by ~70% (data not shown), similar to the previously reported response in rat cortical neurons (18). Fig. 4*E* demonstrates that at least 90% of the remaining KB-R7943-independent Ca^{2+} flux into wild-type neurons was dependent on K^+, confirming that this uptake corresponded to NCKX activity. Similar results were obtained for cells from knock-out animals (data not shown). Fig. 4 shows that the KB-R7943-independent rate of rise in $[Ca^{2+}]_i$ was significantly lower in the cultured neurons from the *nckx2*(−/−) animals compared with matched *nckx2*(+/+) controls (13 ± 2 μM/min and 23 ± 2 μM/min, respectively; $n = 15$, $p < 0.01$). This reduction in Ca^{2+} flux was consistent with the lack of compensatory changes in other Ca^{2+} transport systems. Thus NCKX2 made a major contribution to overall K^+-dependent Na^+/Ca^{2+}-exchange activity, with the remainder being due, presumably, to the activity of NCKX3 and NCKX4. In view of these data, it seemed likely that Ca^{2+} homeostasis in neurons from the *nckx2*(−/−) animals would be significantly impaired.

Hippocampal Synaptic Plasticity—Hippocampal long term potentiation (LTP) at the Schaffer collateral/CA1 pyramidal cell synapse is a classic measure of synaptic plasticity that is critically dependent upon precise control of $[Ca^{2+}]$ (40). NCKX2 transcripts are abundant in CA1 pyramidal neurons (39) and localized to synaptic sites (see Fig. 2). Thus we measured excitatory post-synaptic field potentials (fEPSPs) in the CA1 region arising from stimulation of Schaffer collateral fibers. As illustrated in Fig. 5*A*, the relation between stimulus intensity and fEPSP response was not different between wild-type and knock-out animals, indicating that basal synaptic transmission was not altered by lack of NCKX2 expression. Nor was there any difference in facilitation measured with a paired-pulse protocol, implying that NCKX2, in contrast to NCX2 (16), had no measurable influence on presynaptic $[Ca^{2+}]$ at Schaffer collateral/CA1 pyramidal neuron synapses (Fig. 5*B*).

LTP was induced at the Schaffer collateral/CA1 pyramidal neuron synapses by tetanic stimulation consisting of two 0.5-s trains of 100-Hz stimulation. As illustrated in Fig. 5*C*, there was a profound and highly significant reduction in the extent of LTP in the *nckx2*(−/−) animals compared with the wild-type controls 30 min following induction (88 ± 5% of baseline for knock-out and 131 ± 13% of baseline for wild-type, respectively; $n = 13–15$; $p < 0.01$; see Fig. 5*D*). A critical step in the development of LTP is thought to be Ca^{2+} influx through NMDA-type glutamate receptors subsequent to a depolarization-induced relief of Mg^{2+} block (40). The loss of NCKX2 function might modulate membrane potential via Ca^{2+}-activated K^+ channels (41), thus leading to membrane hyperpolarization, and loss of LTP. This hypothesis was tested in the LTP protocol by two manipulations: either an increase in external $[K^+]$ from 2.5 to 5.5 mM, which would be expected to depolarize neurons by ~20 mV, or a reduction in bath $[Mg^{2+}]$ from 2 mM to 0.25 mM, which would be expected to relieve partially the block of NMDA receptor channels (42). Previous studies demonstrated that these changes in $[K^+]$ and $[Mg^{2+}]$, applied under the stimulation protocol used here, had little or no stimulatory effect on LTP in wild-type hippocampal slices (43–46). When applied to hippocampal slices from *nckx2* knock-out animals, as illustrated in Fig. 5 (*E* and *F*), bath application of raised $[K^+]$ or lowered $[Mg^{2+}]$ both resulted in partial restoration of LTP (summarized in Fig. 5*D*).

Different spatiotemporal patterns of Ca^{2+} signaling are thought to shift the balance between different forms of synaptic plasticity. An abrupt large magnitude change in $[Ca^{2+}]_i$ is thought to promote potentiation (LTP), whereas sustained lower magnitude elevations in $[Ca^{2+}]_i$

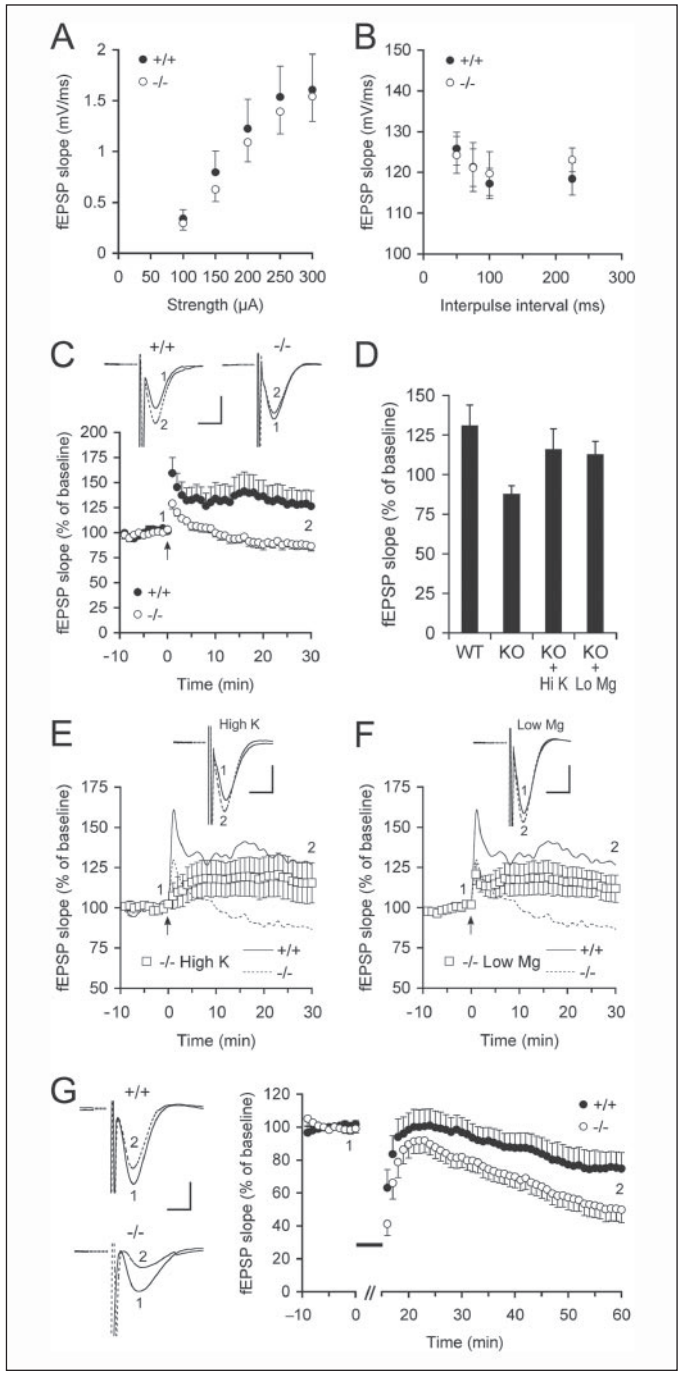

FIGURE 5. **Excitatory post-synaptic potential field recordings (fEPSP) and synaptic plasticity at hippocampal Schaffer/CA1 synapses.** *A*, stimulus intensity *versus* synaptic response for slices from *nckx2* wild-type (+/+) and knock-out (−/−) mice ($n = 7$ or 8 slices from 4 mice of each genotype). *B*, paired pulse protocol ($n = 8$ slices from 4 mice of each genotype). *C*, LTP was elicited in hippocampal slices by two 0.5-s 100-Hz trains given at time = 0 (*arrow*). Averaged traces are shown at the *top* from the indicated time points, and the combined data are plotted below, averaged over 1-min intervals, collected from 13–15 slices from 8 animals of each genotype. *Scale bars* indicate 0.5 mV and 2 ms. *D*, summary graph of the fEPSP data at time point 2 (30 min following stimulation) obtained from *C*, *E*, and *F*. The difference between wild-type (*WT*) and knock-out (*KO*) is statistically significant at $p < 0.01$. *E* and *F*, LTP was induced in hippocampal slices from *nckx2*(−/−) knock-out animals as described in *C*, except that several minutes prior to the experimental recording the bathing medium was replaced with buffer in which either KCl was increased from 2.5 mM to 5.5 mM (*E*) or $MgCl_2$ was reduced from 2 mM to 0.25 mM (*F*). Averaged data are presented from 11 slices from 6 animals in each group. The data from *C* are reproduced as solid (wild-type) and dashed (knock-out) lines for comparative purposes. *G*, LTD was induced in hippocampal slices with a 15-min train of 1 Hz stimulation (*solid bar*). fEPSP data are presented as described for *C*, collected from 12 slices from 6 animals of each genotype. The difference between wild-type and knock-out at time point 2 is statistically significant at $p < 0.05$.

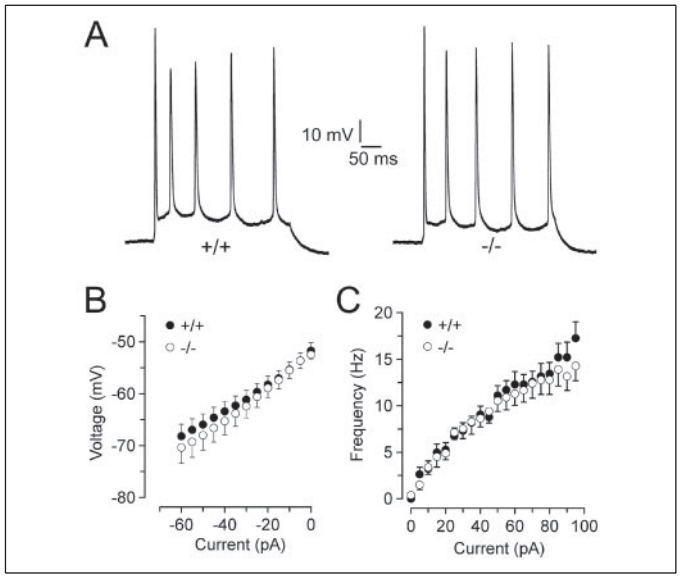

FIGURE 6. **Whole-cell current-clamp analysis of CA1 pyramidal neurons.** *A*, typical traces recorded from CA1 pyramidal neurons of *nckx2* wild-type (+/+) or knock-out (−/−) animals in response to injection of 70 pA of current. *B*, membrane potential is plotted against injected current over the range −60 to 0 pA ($n = 9$ for wild-type (+/+) and $n = 7$ for knock-out (−/−)). *C*, action potential spike frequency is plotted against injected current over the range 0 to 95 pA, as described above.

lead to depression (LTD) (2, 47). Because loss of NCKX2 function abolished LTP at Schaffer collateral/CA1 pyramidal synapses, we examined the development of LTD in wild-type and knock-out animals. Fig. 5*G* illustrates that *nckx2*(−/−) animals displayed enhanced LTD 45 min following its induction in response to 15 min of 1-Hz stimulation of Schaffer collateral/CA1 pyramidal synapses (49.7 ± 7.7% of baseline for the knock-out compared with 74.8 ± 9.7% of baseline for the wild-type; $n = 12$; $p < 0.05$).

To rule out the possibility that the dramatic changes in plasticity observed in *nckx2*(−/−) mice were due to Ca^{2+}-induced failure of CA1 pyramidal neurons to respond to EPSP signals, we used whole-cell current-clamp to analyze these cells. There were no significant differences between wild-type and knock-out animals with respect to resting membrane potential (−51 ± 4 mV for wild type ($n = 9$) and −51 ± 4 mV for knock-out ($n = 7$)), input resistance (244 ± 20 MΩ for wild-type ($n = 9$) and 280 ± 38 MΩ for knock-out ($n = 7$)), values consistent with measurements from CA1 cells maintained in synaptic blockers (48). Similarly, there was no change in action potential spike firing frequency nor in the measured spike parameters (rate of rise, amplitude, half-maximal peak width, or rate of decay; data not shown), as illustrated in Fig. 6. Loss of NCKX2 function was thus without significant effect on parameters that influence the activity of voltage-dependent ion channels in somatic membranes of CA1 pyramidal neurons. These observations are in keeping with the location of NCKX2 expression, which is largely restricted to non-somatic sites (see Fig. 2). In sum, these data support a critical role for NCKX2 in maintaining normal post-synaptic dynamic Ca^{2+} homeostasis at dendritic sites required for proper long term post-synaptic plasticity in hippocampal CA1 pyramidal neurons.

Behavioral Analysis—Changes in synaptic plasticity in the hippocampus are thought to represent cellular mechanisms associated with spatial memory and learning (49). Thus, *nckx2* knock-out mice were subjected to a survey of various tasks designed to assess different aspects of behavior (36, 50). Specific behavioral deficits were observed in both the accelerating rotating rod (rotarod) and Morris water maze tasks. The knock-out mice first displayed normal performance in the rotarod task but were unable to improve their performance with time, in

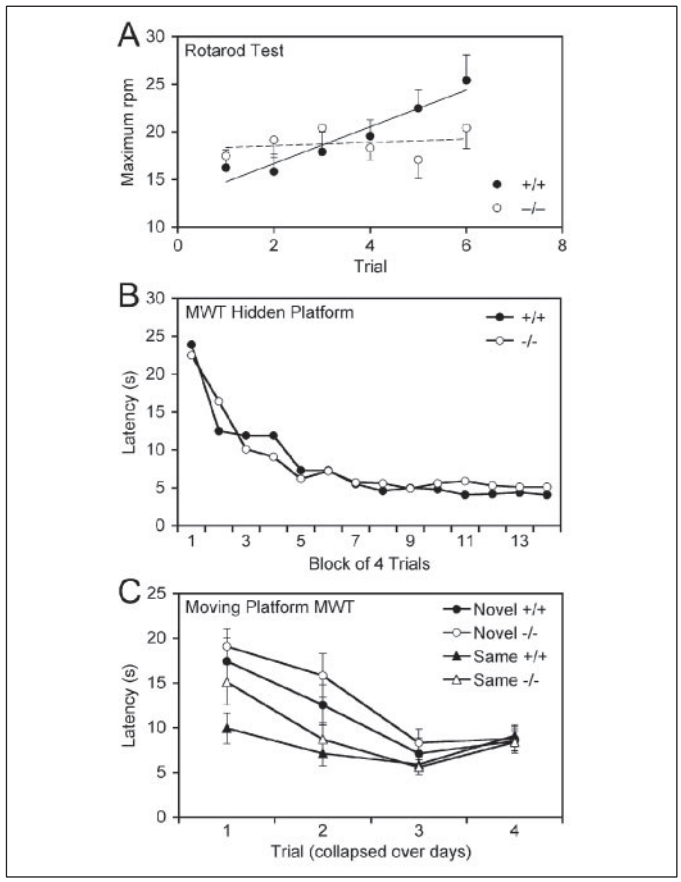

FIGURE 7. **Behavioral analysis of *nckx2* wild-type (+/+) and knock-out (−/−) mice.** *A*, motor learning was tested with the accelerating rotating rod (rotarod) test. The average speed of rotation at which the mice fell off is plotted against trial number (3 trials per day for 2 days). The *lines* are linear regression plots for wild-type (*solid*) and knock-out (*dashed*). The trial *versus* group interaction is statistically significant, $p < 0.03$, indicating a deficit in the ability of the knock-out mice to improve their performance, compared with the wild type. *B*, spatial learning was tested with the Morris water maze task. The mean time required for the mice to find the fixed hidden platform (latency) is plotted against trial block (2 blocks of 4 trials per day for 7 days). There is no difference between genotypes in their ability to learn this task. *C*, spatial working memory was tested using the alternating moving platform version of the Morris water maze task. Data were averaged over days where the platform was either in the same position as the previous day, or in a novel location. The average time taken to find the platform (latency) is plotted against the trial. Wild-type mice showed a benefit from the previous day's experience and found the platform in the same location on the first trial faster than knock-out, and faster than when the platform was in a novel location ($p < 0.05$). There is also a statistically significant group *versus* trial interaction ($p < 0.01$).

contrast to the improvement seen with wild-type animals. This difference was statistically significant as demonstrated by the interaction between group and trial ($p = 0.03$) and illustrated in Fig. 7*A*. In the Morris water maze task, both groups of animals showed improved performance in their ability to find the fixed hidden platform (Fig. 7*B*). In the moving platform version of this task, wild-type mice showed a significant improvement in their performance on the first trial when the platform was in the same location as the previous day, compared with when it was in a novel location. The *nckx2* knock-out mice, on the other hand, did not show similar improvement. This difference was evident as a statistically significant interaction between group and trial ($p = 0.007$).

There was also a difference, although only at the borderline of significance, in the open field test, a task that assesses habituation to a novel environment. When placed into the chamber wild-type mice were observed to travel a shorter distance and to rear up more often over time, whereas the behavior of knock-out mice changed less (the group *versus* time interaction for distance traveled displayed $p = 0.057$, and for rears, $p = 0.05$). It is important to note that in all three of these behav-

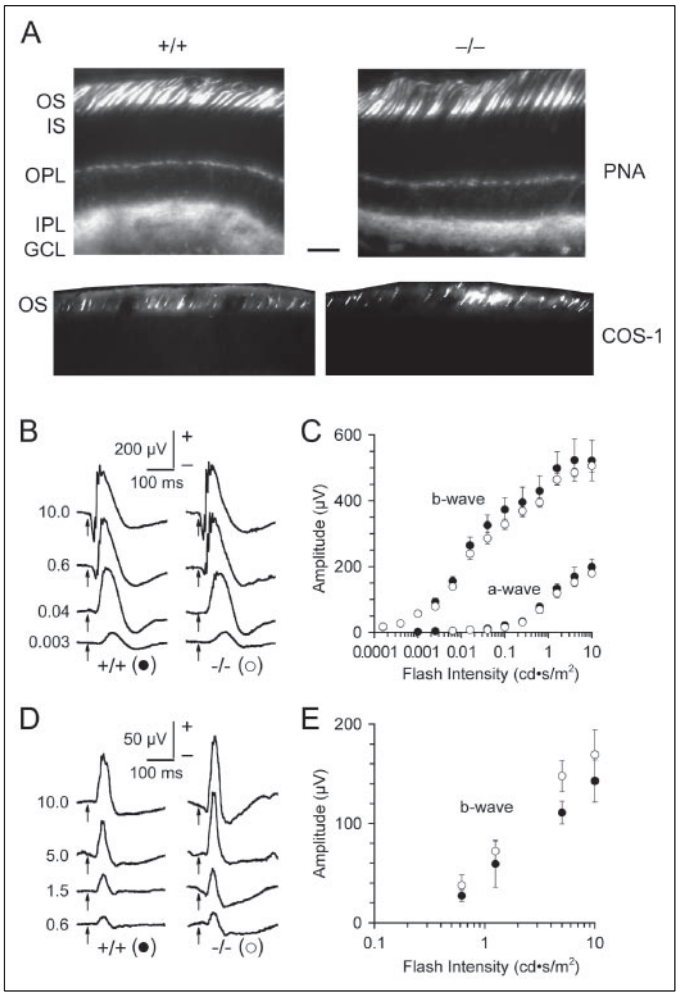

FIGURE 8. **Photoreceptor morphology and function.** *A*, cryostat cross-sections of retina from *nckx2* wild-type (+/+) or knock-out (−/−) mice were labeled with peanut agglutinin or with the COS-1 antibody to visualize cones. *OS*, outer segment layer; *IS*, inner segment layer; *OPL*, outer plexiform layer; *IPL*, inner plexiform layer; *GCL*, granule cell layer. Photographs are representative of several fields from 4 or 5 animals of each genotype. *Scale bar*, 50 μm. *B*, representative sample electroretinography traces recorded under scotopic conditions for *nckx2* wild-type (+/+) and knock-out (−/−) mice are shown. The *arrows* indicate the onset of the light flash of intensity indicated to the *left* of *each trace* (in cd•s/m^2). *C*, intensity-response data are plotted for the a- and b-waves obtained from recordings like those shown in *B* ($n = 6$ for each genotype). *Filled symbols*, wild-type; *open symbols*, knock-out. *D* and *E*, sample electroretinography traces and summary intensity-response data for the derived b-waves are shown for recordings obtained under photopic conditions (prior exposure to light of intensity 32 cd/m^2), as described above.

ioral tests initial performance of the knock-out mice was indistinguishable from that of control; it was only following a persistent benefit from experience that the control mice demonstrated performance superior to that of the knock-out mice. These data indicate that the loss of control of local Ca^{2+} homeostasis in the *nckx2*(−/−) mice causes very specific deficits in experience-dependent learning tasks.

No other significant trends or differences were observed between the wild-type and knock-out groups with respect to general appearance, health, or reflexes; visual, auditory, gustatory, or tactile perception; general motor function or balance; circadian rhythm; anxiety; nor in certain memory-related tasks such as contextual fear conditioning, fear-potentiated startle, or simple spatial learning.

Retina and Vision—In addition to expression in brain (39), *nckx2* has been cloned from chicken and human retina and reported to be enriched in cone photoreceptors (51, 52). Loss of the major Ca^{2+} extrusion system from cone outer segments would be expected to lead to Ca^{2+} overload and subsequent photoreceptor degeneration. Cone abundance, assessed by staining comparably oriented retinal sections either with peanut agglutinin, which labels the sheaths of all cones (33), or with monoclonal antibody COS-1, which recognizes M/L cones (32), was not different between wild-type and knock-out animals, as illustrated in Fig. 8*A* (14 ± 1 *versus* 14 ± 1 cones/100 μm for peanut agglutinin staining, and 11 ± 1 *versus* 11 ± 1 cones/100 μm for COS-1 staining, in wild-type *versus* knock-out animals, respectively).

Furthermore, visual function assessed by electroretinography was not different between the wild-type and knock-out animals (Fig. 8, *B–E*). Importantly, the responses to light over the 1–10 cd•s/m^2 range of illumination intensity, as well as all recordings performed with a rod-saturated background, increased similarly for *nckx2* wild-type and knock-out animals, although the response would have been expected to be flat in the absence of cone function (53). There is thus no obvious loss of cone number nor any major deficit in their response to illumination in the *nckx2*(−/−) animals. These data suggest that the NCKX2 protein is not essential for cone development, viability, or visual transduction, although a more subtle role for this exchanger in cone function is not ruled out.

DISCUSSION

Since the discovery that several different members of the K^+-dependent Na^+/Ca^{2+}-exchanger (NCKX) family are broadly expressed in brain neurons (17) and contribute significantly to Ca^{2+} flux (8, 19–21), the specific role subserved by these different proteins has been a key unresolved question. Deletion of the NCKX2 protein in mice has now allowed examination of the specific role this molecule plays in neuronal physiology. The major conclusions from this work are that NCKX2 is essential for the control of local Ca^{2+} homeostasis that is required for the development of normal synaptic plasticity in hippocampal neurons and is also required for specific experience-related learning tasks. On the other hand, NCKX2 is not required for cone photoreceptor development, maintenance or operation in mice.

Our data demonstrate a significant contribution of NCKX2 to the KB-R7943-insensitive Ca^{2+} flux in cortical neurons, as would be expected from the high levels of *nckx2* expression observed in these cells (39). The individual cell trace data shown in Fig. 4 (*A* and *B*) indicate that, for most neurons, loss of NCKX2 leads to a reduction, rather than an abolition, of K^+-dependent Ca^{2+} uptake, suggesting that multiple NCKX isoforms are likely to be present in many neurons. This redundancy, however, is not sufficient to compensate for the loss of NCKX2 function, at least with respect to the induction of LTP and the enhancement of LTD that we observed at Schaffer collateral/CA1 pyramidal neuron synapses.

Although NCKX2 makes a contribution of >40% to K^+-dependent Ca^{2+} flux (Fig. 4), its contribution to overall Ca^{2+} flux that includes NCX-type exchangers is only ~10–15%. This relatively modest contribution seems at odds with the dramatic and robust effect that loss of NCKX2 function has on synaptic plasticity (Fig. 5). We believe the disproportionate contribution of NCKX2 to Ca^{2+} flux compared with synaptic plasticity can be explained by a combination of spatially localized expression and specific kinetic properties.

The Ca^{2+} flux experiments performed here were done on whole cells, hence integrating the activities of all surface-expressed functional transporters. On the other hand, our immunolocalization data in hippocampus (Fig. 2) revealed selective expression of NCKX2 in neuronal processes away from the cell body. The contribution of NCKX2 to Ca^{2+} flux and homeostasis at these restricted sites may be much larger. In support of this argument, previous studies examining Ca^{2+} flux sug-

gested up to 60% contribution by K^+-dependent Na^+/Ca^{2+}-exchangers in isolated nerve terminal preparations but a much smaller contribution at the cell soma (19–21). Furthermore, the activity of membrane transporters is determined by the local concentrations of ions and the affinity with which they bind and are transported. These parameters differ between different NCX and NCKX isoforms, so that each may only contribute to Ca^{2+} flux under certain conditions.

One of the striking findings of our study is that loss of NCKX2 function in *nckx2* knock-out animals lead to loss of hippocampal LTP and enhancement of LTD (Fig. 5). This result is opposite from previous findings in *ncx2* knock-out mice, where loss of the NCX2 protein lead to an enhancement in LTP and a shift away from LTD (16). How can the loss of two proteins that both function to extrude Ca^{2+} lead to opposite effects on synaptic plasticity? We consider two possible explanations, which in fact may both contribute partially, for the dichotomy of function between NCX2 and NCKX2: location and kinetics.

Differences in post-synaptic Ca^{2+} dynamics are thought to be critical in underlying the balance between processes that promote LTP *versus* those that promote LTD (2, 47). Large but brief increases in $[Ca^{2+}]$ lead to LTP, via the activation of Ca^{2+}-calmodulin-dependent kinase II, as well as other protein kinases. On the other hand, lower magnitude changes in $[Ca^{2+}]$ that are sustained for longer periods of time lead to the activation of phosphatases such as calcineurin. NCX2 has high activity that is allosterically regulated by cytosolic Ca^{2+} with a half-maximal concentration of ~1.5 μM (54). NCX2 would therefore be expected to play a predominant role in Ca^{2+} extrusion only when $[Ca^{2+}]$ levels are significantly elevated. As $[Ca^{2+}]$ falls lower, NCX2 will turn off, and other pathways for Ca^{2+} extrusion will take over. Loss of NCX2 would therefore be expected to result in higher peak values of post-synaptic Ca^{2+} transients, the net result being a shift toward LTP. NCKX2, on the other hand, is not allosterically modulated by cytosolic Ca^{2+} (55) and is activated at lower $[Ca^{2+}]$ (<1 μM (56)) than is NCX2. These values suggest that NCKX2 would contribute more significantly to $[Ca^{2+}]$ homeostasis following a transient spike and that loss of NCKX2 function might lead to a sustained enhancement of $[Ca^{2+}]$, which would promote LTD.

It is likely that subcellular localization plays an important part in defining the different physiological roles for NCX2 and NCKX2 proteins. Our data presented in Fig. 2 demonstrate a selective expression of the NCKX2 protein in neuronal processes rather than the cell soma. This localization is supported functionally both by previous studies using nerve terminal preparations (19–21) and by our data showing no change in various somatic membrane electrical properties or cell excitability parameters between *nckx2* wild-type and knock-out CA1 pyramidal neurons (Fig. 6). Immunocytochemical localization studies on NCX2, however, demonstrated a preferential localization to the cell soma (14). Additional support for differential functional expression of NCX2 compared with NCKX2 comes from the paired-pulse protocol used to measure pre-synaptic facilitation. Although we found no effect of NCKX2 loss on this parameter (Fig. 5*B*), loss of NCX2 has a dramatic effect on paired pulse facilitation (16).

Taken together, these data suggest that loss of NCX2 may selectively influence somatic Ca^{2+} homeostasis, whereas loss of NCKX2 may preferentially influence dendritic Ca^{2+} homeostasis (because NCKX2 is present in neuronal processes, but not presynaptic sites, in the hippocampus). Alterations in Ca^{2+} clearance as a consequence of the loss of NCKX2 function may cause activation of Ca^{2+}-sensitive K^+-channels. Hippocampal CA1 neurons express both small- (SK) and high- (BK) conductance Ca^{2+}-activated K^+-channels (57). Within dendrites, BK channels tend to be excluded (58), whereas SK channels present at dendritic spines are responsible for local membrane repolarization (59). SK channels thus mediate a Ca^{2+}-dependent feedback inhibition on NMDA-receptor channel function (48). Enhanced activation of SK channels consequent to the reduction in localized Ca^{2+} efflux in *nckx2* knock-out animals would result in more rapid re-polarization of dendritic spine membrane potentials. This change would both reduce the likelihood of propagating a dendritic membrane depolarization and inhibit activation of NMDA receptors induced by tetanic stimulation. Such effects would lead to the loss of LTP at the Schaffer collateral/CA1 pyramidal cell synapse, as we observe in the *nckx2*(−/−) mice (Fig. 5). This hypothesis is supported by the partial recovery of LTP either by mild depolarization (elevated bath $[K^+]$), or by reducing Mg^{2+}-blockade of NMDA receptors (lowered bath $[Mg^{2+}]$) seen in Fig. 5 (*D–F*). To what extent changes in localized Ca^{2+} signaling or differences in Ca^{2+} efflux kinetics contribute to the differences observed in synaptic plasticity in *ncx2 versus nckx2* knock-out mice clearly requires further investigation.

The strong effect of *nckx2* knock out on hippocampal CA1 LTP would predict deficits in spatial learning, as measured by the Morris water maze task. Surprisingly, however, wild-type and knock-out mice demonstrated identical improvements in their performance with the number of trials on the standard hidden platform version of this task (Fig. 7*B*). Only in the modified moving platform version of the task were deficits observed for the *nckx2*(−/−) mice. Similar observations of a dissociation between hippocampal LTP and spatial learning have been reported previously in mice lacking the AMPA receptor subunit GluR1 (60). Our data thus suggest that *nckx2* knock-out mice express a deficit in spatial working memory but not reference memory, or possibly a deficit in memory consolidation or retention. Our observation that hippocampal LTD was enhanced in the *nckx2*(−/−) mice is also consistent with a deficit in memory consolidation or retention.

Our observations of a deficit in motor learning in the rotarod test between *nckx2* knock-out and wild-type mice are consistent with an important role for NCKX2 within the cerebellum. We did not test plasticity at cerebellar synapses in this study. However, NCKX2 is known to be expressed abundantly both in neurons of the deep cerebellar nuclei and in inhibitory interneurons of the cerebellar molecular layer (39). These cerebellar circuits are believed to be important for motor learning (61, 62), and it seems likely that the loss of NCKX2 function at these sites might induce similar alterations in Ca^{2+} homeostasis important for synaptic plasticity as we observed in hippocampal CA1 neurons. This concept warrants further investigation.

Rod and cone photoreceptors mediate visual function in low and bright ambient light conditions, respectively, and cone-dependent pathways allow color vision. Rods and cones are generally thought to employ similar visual signaling cascades, although the set of protein used in rods is replaced with a parallel set, encoded by different, but homologous, genes in cones (63). In rods, the $Na^+/(Ca^{2+}+K^+)$-exchanger, NCKX1, is known to play a critical role in maintaining normal calcium homeostasis, especially in the dark when Ca^{2+} influx through open cyclic nucleotide-gated channels is high. NCKX1 is the only Ca^{2+} efflux pathway in the rod outer segment, and so loss of its function would rapidly lead to Ca^{2+} overload, the activation of degradative enzymes, and, subsequently, degenerative loss of rod photoreceptors (64). Because NCKX2 has been reported to be expressed in cone photoreceptors (51, 52), loss of its function would be expected to lead to cone degeneration. Surprisingly, *nckx2*(−/−) mice do not display any obvious deficit either in the number of cones nor in their function in adult animals. This result suggests that either NCKX2 is not the major pathway for Ca^{2+} extrusion in mouse cone photoreceptors, or other

transport pathways must compensate for the loss of NCKX2 function at this site. Clearly the nature of the Ca^{2+} efflux pathway from cone photoreceptors needs further investigation.

Our studies reported here demonstrate a unique role for NCKX2-mediated Ca^{2+} efflux that is dramatically distinct from that found previously for NCX2 (16). These observations highlight the non-redundant properties and physiological connections of different Ca^{2+} extrusion mechanisms and suggest that new fundamental insights into the local control of Ca^{2+} signaling and its importance in neuronal function will come from further studies on these transport proteins.

Acknowledgments—We thank Dr. W. Stell (University of Calgary) for the gift of COS-1 antibody and for helpful advice and critical comments on the manuscript, Dr. B. Kuzmiski (University of Calgary) for assistance in establishing brain slice field recordings, Drs. B. Quednau and K. Philipson (UCLA) for the gift of rat NCX2 cDNA, S. Leach, K. Zhang, and Y. Wang for technical assistance, and the journal referees who provided suggestions that have been incorporated into the "Discussion" of this report.

REFERENCES

1. Berridge, M. J., Lipp, P., and Bootman, M. D. (2000) *Nat. Rev. Mol. Cell Biol.* **1,** 11–21
2. Augustine, G. J., Santamaria, F., and Tanaka, K. (2003) *Neuron.* **40,** 331–346
3. Berridge, M. J., Bootman, M. D., and Roderick, H. L. (2003) *Nat. Rev. Mol. Cell Biol.* **4,** 517–529
4. Blaustein, M. P., and Lederer, W. J. (1999) *Physiol. Rev.* **79,** 763–854
5. Choi, D. W. (2005) *Nature* **433,** 696–698
6. Bano, D., Young, K. W., Guerin, C. J., Lefeuvre, R., Rothwell, N. J., Naldini, L., Rizzuto, R., Carafoli, E., and Nicotera, P. (2005) *Cell* **120,** 275–285
7. Pignataro, G., Tortiglione, A., Scorziello, A., Giaccio, L., Secondo, A., Severino, B., Santagada, V., Caliendo, G., Amoroso, S., Di Renzo, G., and Annunziato, L. (2004) *Neuropharmacology* **46,** 439–448
8. Kiedrowski, L., Czyz, A., Baranauskas, G., Li, X. F., and Lytton, J. (2004) *J Neurochem.* **90,** 117–128
9. Li, S., Jiang, Q., and Stys, P. K. (2000) *J. Neurophysiol.* **84,** 1116–1119
10. Imahashi, K., Pott, C., Goldhaber, J. I., Steenbergen, C., Philipson, K. D., and Murphy, E. (2005) *Circ. Res.* **97,** 916–921
11. Cai, X., and Lytton, J. (2004) *Mol. Biol. Evol.* **21,** 1692–1703
12. Quednau, B. D., Nicoll, D. A., and Philipson, K. D. (2004) *Pflügers Arch.* **447,** 543–548
13. Schnetkamp, P. P. (2004) *Pflügers Arch.* **447,** 683–688
14. Papa, M., Canitano, A., Boscia, F., Castaldo, P., Sellitti, S., Porzig, H., Taglialatela, M., and Annunziato, L. (2003) *J. Comp. Neurol.* **461,** 31–48
15. Reuter, H., and Porzig, H. (1995) *Neruon* **15,** 1077–1084
16. Jeon, D., Yang, Y. M., Jeong, M. J., Philipson, K. D., Rhim, H., and Shin, H. S. (2003) *Neuron.* **38,** 965–976
17. Lytton, J., Li, X. F., Dong, H., and Kraev, A. (2002) *Ann. N. Y. Acad. Sci.* **976,** 382–393
18. Kiedrowski, L. (2004) *Neuroreport* **15,** 2113–2116
19. Lee, S. H., Kim, M. H., Park, K. H., Earm, Y. E., and Ho, W. K. (2002) *J. Neurosci.* **22,** 6891–6899
20. Kim, M. H., Lee, S. H., Park, K. H., and Ho, W. K. (2003) *J. Neurosci.* **23,** 11673–11680
21. Kim, M. H., Korogod, N., Schneggenburger, R., Ho, W. K., and Lee, S. H. (2005) *J. Neurosci.* **25,** 6057–6065
22. Tsuzuki, T., and Rancourt, D. E. (1998) *Nucleic Acids Res.* **26,** 988–993
23. Marth, J. D. (1996) *J. Clin. Invest.* **97,** 1999–2002
24. Lees-Miller, J. P., Guo, J., Somers, J. R., Roach, D. E., Sheldon, R. S., Rancourt, D. E., and Duff, H. J. (2003) *Mol. Cell Biol.* **23,** 1856–1862
25. Ausubel, F. M., Brent, R., Kingston, R. E., Moore, D. D., Seidman, J. G., Smith, J. A., and Struhl, K. (eds). (2005) *Current Protocols in Molecular Biology*, John Wiley & Sons, New York, NY
26. Wu, K.-D., and Lytton, J. (1993) *Am. J. Physiol.* **264,** C333–C341
27. Salvaterra, P. M., and Matthews, D. A. (1980) *Neurochem. Res.* **5,** 181–195
28. Laemmli, U. K. (1970) *Nature* **227,** 680–685
29. Cai, X., Zhang, K., and Lytton, J. (2002) *J. Biol. Chem.* **277,** 48923–48930
30. Porzig, H., Li, Z., Nicoll, D. A., and Philipson, K. D. (1993) *Am. J. Physiol.* **265,** C748–C756
31. Chandrasekera, C. P., and Lytton, J. (2003) *J. Biol. Chem.* **278,** 12482–12488
32. Szel, A., Rohlich, P., Caffe, A. R., and van Veen, T. (1996) *Microsc. Res. Tech.* **35,** 445–462
33. Blanks, J. C., and Johnson, L. V. (1983) *J. Comp. Neurol.* **221,** 31–41
34. Czyz, A., and Kiedrowski, L. (2002) *J. Neurochem.* **83,** 1321–1328
35. Kiedrowski, L., and Czyz, A. (2002) *Ann. N. Y. Acad. Sci.* **976,** 413–417
36. Whishaw, I. Q., Haun, F., and Kolb, B. (1999) in *Modern Techniques in Neuroscience Research* (Windhorst, U., and Johansson, H., eds) pp. 1243-1271, Springer, Berlin
37. Tremblay, F., Abdel-Majid, R., and Neumann, P. E. (2002) *Vision Res.* **42,** 1715–1725
38. Sharon, D., Yamamoto, H., McGee, T. L., Rabe, V., Szerencsei, R. T., Winkfein, R. J., Prinsen, C. F., Barnes, C. S., Andreasson, S., Fishman, G. A., Schnetkamp, P. P., Berson, E. L., and Dryja, T. P. (2002) *Invest. Ophthalmol. Vis. Sci.* **43,** 1971–1979
39. Tsoi, M., Rhee, K.-H., Bungard, D., Li, X.-F., Lee, S.-L., Auer, R. N., and Lytton, J. (1998) *J. Biol. Chem.* **273,** 4115–4162
40. Lynch, M. A. (2004) *Physiol. Rev.* **84,** 87–136
41. Wann, K. T., and Richards, C. D. (1994) *Eur. J. Neurosci.* **6,** 607–617
42. Dingledine, R., Borges, K., Bowie, D., and Traynelis, S. F. (1999) *Pharmacol. Rev.* **51,** 7–61
43. Ballyk, B. A., and Goh, J. W. (1992) *J. Neurosci. Res.* **33,** 598–604
44. Huang, Y. Y., Wigstrom, H., and Gustafsson, B. (1987) *Neuroscience* **22,** 9–16
45. Poolos, N. P., and Kocsis, J. D. (1990) *Brain Res.* **508,** 7–12
46. Stringer, J. L., and Lothman, E. W. (1988) *Exp. Neurol.* **101,** 147–157
47. Malenka, R. C., and Bear, M. F. (2004) *Neuron.* **44,** 5–21
48. Ngo-Anh, T. J., Bloodgood, B. L., Lin, M., Sabatini, B. L., Maylie, J., and Adelman, J. P. (2005) *Nat. Neurosci.* **8,** 642–649
49. Eichenbaum, H. (2004) *Neuron* **44,** 109–120
50. Crawley, J. N. (1999) *Brain Res.* **835,** 18–26
51. Prinsen, C. F., Szerencsei, R. T., and Schnetkamp, P. P. M. (2000) *J. Neurosci.* **20,** 1424–1434
52. Prinsen, C. F., Cooper, C. B., Szerencsei, R. T., Murthy, S. K., Demetrick, D. J., and Schnetkamp, P. P. (2002) *Adv. Exp. Med. Biol.* **514,** 237–251
53. Biel, M., Seeliger, M., Pfeifer, A., Kohler, K., Gerstner, A., Ludwig, A., Jaissle, G., Fauser, S., Zrenner, E., and Hofmann, F. (1999) *Proc. Natl. Acad. Sci. U. S. A.* **96,** 7553–7557
54. Li, Z., Matsuoka, S., Hryshko, L. V., Nicoll, D. A., Bersohn, M. M., Burke, E. P., Lifton, R. P., and Philipson, K. D. (1994) *J. Biol. Chem.* **269,** 17434–17439
55. Dong, H., Light, P. E., French, R. J., and Lytton, J. (2001) *J. Biol. Chem.* **276,** 25919–25928
56. Sheng, J. Z., Prinsen, C. F., Clark, R. B., Giles, W. R., and Schnetkamp, P. P. M. (2000) *Biophys. J.* **79,** 1945–1953
57. Sah, P. (1996) *Trends Neurosci.* **19,** 150–154
58. Poolos, N. P., and Johnston, D. (1999) *J. Neurosci.* **19,** 5205–5212
59. Cai, X., Liang, C. W., Muralidharan, S., Kao, J. P., Tang, C. M., and Thompson, S. M. (2004) *Neuron.* **44,** 351–364
60. Reisel, D., Bannerman, D. M., Schmitt, W. B., Deacon, R. M., Flint, J., Borchardt, T., Seeburg, P. H., and Rawlins, J. N. (2002) *Nat. Neurosci.* **5,** 868–873
61. Medina, J. F., Repa, J. C., Mauk, M. D., and LeDoux, J. E. (2002) *Nat. Rev. Neurosci.* **3,** 122–131
62. Nakanishi, S. (2005) *Trends Neurosci.* **28,** 93–100
63. Korenbrot, J. I., and Rebrik, T. I. (2002) *Adv. Exp. Med. Biol.* **514,** 179–203
64. Schnetkamp, P. P. M. (1995) *Cell Calcium* **18,** 322–330